Available online at www.sciencedirect.com

ScienceDirect

Advances in Space Research 75 (2025) 767–778

ADVANCES IN SPACE RESEARCH (a COSPAR publication)

www.elsevier.com/locate/asr

Design and experimental verification of a robust control to avoid individual calibration of multiple reaction wheels in satellites

K. Olfe, A. Bello, J. Fernández, J. Rodríguez, V. Lapuerta *

E-USOC, Center for Computational Simulation, Escuela Técnica Superior de Ingeniería Aeronáutica y del Espacio, Universidad Politécnica de Madrid, Plaza de Cardenal Cisneros 3, 28040 Madrid, Spain

Received 22 November 2023; received in revised form 17 September 2024; accepted 24 September 2024
Available online 1 October 2024

Abstract

Momentum exchange devices like momentum wheels and reaction wheels are widely used in spacecraft attitude control. Managing their internal momentum, so that it is interchanged with the angular momentum of the rest of the spacecraft, usually involves controlling the angular velocity of these devices. This can be done by characterizing and performing a precise calibration on the wheel. However, this approach has some drawbacks, as small manufacturing differences require characterizing each individual wheel that is used, and the performance of each wheel can suffer small changes through the lifecycle of the satellite. This can be especially laborious in the case of spacecrafts with several reaction wheels, constellation of satellites or, more generally, when a set of reaction wheels are manufactured with the same specifications, since it would require calibrating each of the wheels.

This paper presents a new control design concept that avoids the necessity of calibrating all the wheels by formulating the calibration variations as a disturbance rejection problem, where the errors introduced by the absence of a dedicated calibration curve are treated as an external low frequency noise added to the command velocity, and a H_∞ controller is synthesized to reject it. Experimental results have been obtained with a set of laboratory satellites, showing that the proposed methodology is able to handle out-of-calibration configurations, and improves the performance even when all wheels are well calibrated.

Keywords: Spacecraft attitude; Reaction wheel; Satellite constellation; Robust control; Attitude control; H-infinity control

1. Introduction

Almost all the space missions have some spacecraft pointing or attitude requirements, coming from tumbling margins, imaging or communication constraints, etc. That is why the satellite's Attitude Determination and Control Subsystem (ADCS) performs a crucial task for the success of its mission. Momentum exchange devices, such as reaction wheels, are widely used as actuators to generate the required torques for attitude control. Although reaction wheels have been used in spacecraft control systems for a long time, improving their performance is a problem still relevant (Lobanov et al., 2016; Navabi and Hosseini, 2017) due to the necessity to deal with the degradation of the spacecraft elements and with parametric uncertainty. Moreover, these devices need to manage their stored momentum, adding a new control problem to avoid saturation and maintain their angular velocity within a certain working range. Of course, this is not a straightforward problem and is handled differently depending on the associated software and hardware.

* Corresponding author.
E-mail addresses: ks.olfe@upm.es (K. Olfe), alvaro.bello@upm.es (A. Bello), jose.ffraile@upm.es (J. Fernández), jacobo.rodriguez@upm.es (J. Rodríguez), mariavictoria.lapuerta@upm.es (V. Lapuerta).

https://doi.org/10.1016/j.asr.2024.09.053
0273-1177/

From the software point of view, it is true that the linear attitude controllers were able (if well-tuned) to manage wheels calibration errors. Nevertheless, there are some points to look for a correct functionality of the wheels:

- A correct commanding of the wheels is desirable in any case. From a robust analysis point of view, the commanding errors in the wheel can be seen as a perturbation torque in the control signal. Therefore, even though the attitude controller can handle this perturbation, it will reduce the margin to absorb other perturbations.
- For non-linear controllers, the wheels behavior could be more critical. Fig. 1 is a simulation for fuzzy-logic-based attitude controllers. These controllers have shown very interesting performance in simulations from an error-cost point of view (see (Bello et al., 2021) but may suffer from a lack of robustness. To make the attitude control components robust could be a first step to workaround this issue. The controller used in this simulation is the Low Cost one described in (Bello et al., 2021). A commanding error of 10 % of maximum torque was introduced in the commanding signal and, as a consequence, an attitude steady state error appeared. A 5 degrees slew maneuver was commanded (t = 100 s) and the slope induced by the controller also changed. When the commanding error reduces the torque applied, the slope is lower. A command to recover the original attitude was also introduced in the simulation (at about t = 400 s). In this case the commanding error increase the torque and as a consequence an overshoot appeared.
- The commanding error could complicate the momentum managing and increase the necessity of momentum unloads.
- Last thing is to remark that this approach can be useful for any system using Electronic Speed Controllers with Brushless DC motors, for example in (Desai and Emadi, 2005; de Castro et al., 2018) and (Sathyan et al., 2009).

Regarding the hardware, Fig. 2 shows a typical commanding schema for a reaction wheel attached to a brushless direct current (BLDC) motor (Desai and Emadi, 2005; de Castro et al., 2018) controlled with an Electronic Speed Controller (ESC), typical in satellites. The desired wheel velocity, Ω_{target}, is the result of the ADCS processor calculations to obtain the required torque to control the attitude of the satellite. A calibration curve, implemented also in the ADCS processor, transforms this velocity to a Pulse-Width Modulation (PWM) signal, used by the ESC to set the motor rotation. This is done by commuting the three phases of the motor in a proper way. The ESC requires some type of feedback to set the correct polarity in each phase, for example the back electromotive force (EMF) of each phase (as is represented in Fig. 2) or signals from Hall sensors. Finally, the resulting velocity of the wheel is Ω.

A typical calibration assigns a PWM value for the maximum rotational speed, another PWM value for the minimum rotational speed, and a linear function between those two points. However, those maximum and minimum values can be affected by many factors: design and manufacturing (for example, they will be more predictable if the ADCS and ESC processors have the same external oscillator), environmental factors (specially the temperature), lifetime, etc. Thus, if several wheels are used, even if they are all manufactured in the same way, the same PWM value will drive each wheel to a different angular velocity, and, therefore, each wheel will require a more precise calibration to ensure that the achieved wheel velocity is the commanded one. This can be done through dedicated calibration curves, unique for each wheel and, in addition, a recalibration if possible, during the life of the satellite. However, these processes can require a considerable amount of time if many wheels are used, as for example in a constellation of satellites.

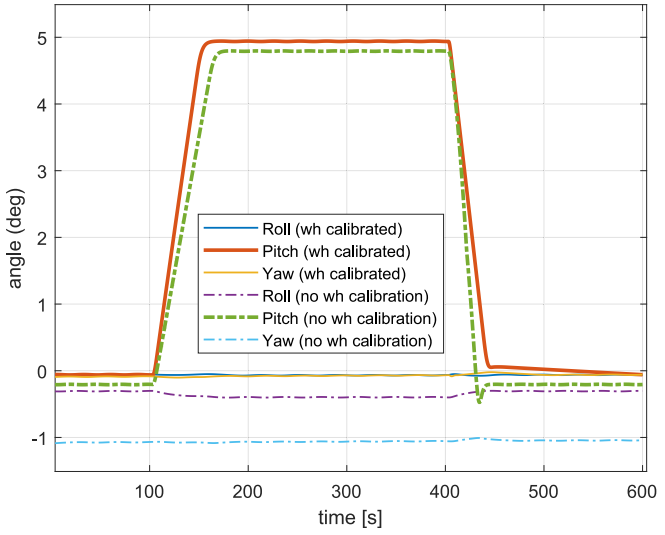

Fig. 1. Simulation of a pitch step maneuver with reaction wheel with and without calibration errors for fuzzy-logic-based attitude controller.

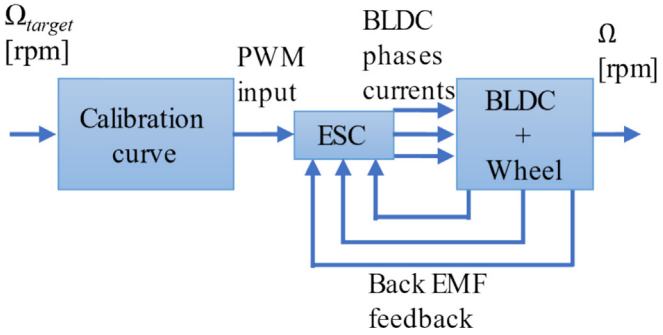

Fig. 2. Wheel commanding schema for a brushless motor driven by an ESC with electromotive force feedback.

Some previous works add a speed feedback control to improve the performance of an individual wheel. For example, to reject disturbances caused by the internal friction of the wheel assembly as in (Ge and Cheng, 2006), or to analyze the behavior during a zero-speed crossing maneuver (Carrara and Kuga, 2015). However, research involving the reaction wheels technology has a commercial interest, so not many works give wheel design details or report performance tests, and even fewer provide details about the wheel controllers. In (Hoevenaars et al., 2012) a discrete model-based PID controller for a reaction wheel based on a BLDC motor was studied numerically for a CubeSat mission. (Fatimi et al., 2022) proposed a software-in-the-loop simulation to analyze the performance of a PID speed control for a reaction wheel. In (Muhamad et al., 2016) a Linear Quadratic Regulator (LQR) for a reaction wheel with a Direct Current (DC) motor was designed to minimize the power consumption of the motor. Reaction wheel controllers based on Fuzzy Logic have also been developed and simulated (Burakov et al., 2019). However, those previous works are focused on the performance of an individual wheel and, if multiple wheels are used, an individual calibration for each wheel is necessary.

In this work, instead of characterizing and calibrating each wheel individually, a single calibration curve is used for all wheels and an external controller is added, which introduces a new control design concept, that is able to handle the mentioned differences between wheels, by formulating the calibration variations as a disturbance rejection problem, where the errors introduced by the absence of a dedicated calibration curve are treated as an external low frequency noise added to the command velocity, and a H_∞ controller (Apkarian and Noll, 2006) is synthesized to reject it. This external controller deals, not only with each individual wheel performance, but also, and more importantly, with the calibration errors and variations between different wheels. And it also avoids future recalibrations along the lifetime of the wheels.

Fig. 3 shows a schema of the wheel commanding with the external controller, C, where Ω_{error} is the difference between the target velocity and the current one and Ω_{cmd} is the velocity commanded by the external controller (the controller output). The external controller design is based on the H_∞ theory (Apkarian and Noll, 2006), which is used to tune a Proportional, Integral, Derivative (PID) (Sidi, 2014).

Once the external controller is presented, ths work shows how to implement the new design control concept in a real hardware and its performance is experimentally tested on a set of laboratory nanosatellites ESAT (Theia Space, 2023).The methodology presented here is extensible to any hardware application where multiple BLDC motors are used, and individual calibrations are to be avoided.

This document is divided as follows: Section 2 presents the detailed theory and calculations used to design the external controller; Section 3 shows the main experimental results; Section 4 is a discussion on the uncertainty in the model; and finally, Section 5 summarizes the conclusions of the work.

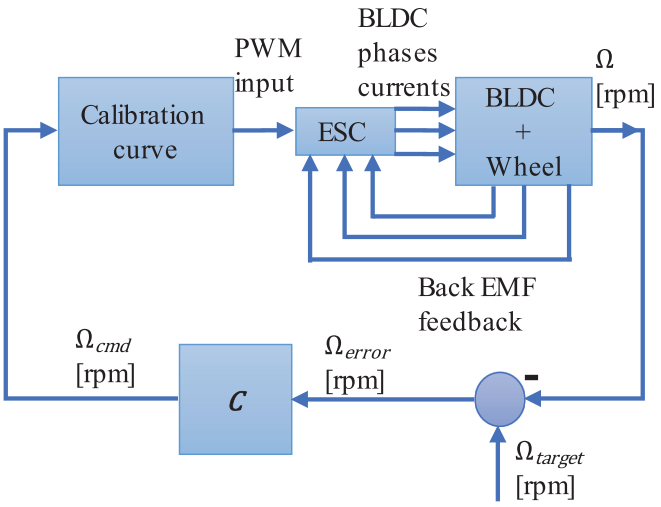

Fig. 3. Wheel commanding schema implemented on board ESAT to have the same calibration curve and controller for the wheels of all the ESATs. C is the external controller.

2. Theory and calculation

The schema used to control each wheel is presented in Fig. 4a).

Fig. 4a) is a reorganization of Fig. 3 where C is the external controller and P is the plant (the wheel with the ESC and the calibration curve, as in Fig. 2). An alternative feedback possibility is present in Fig. 4b). The main difference is that the controller signal is a velocity increment, $\Delta\Omega$, instead of Ω_{cmd}. This schema is very common in feedback control, but finally the one presented in a) was preferred for avoiding multiple calibration of the wheels. This is because the main advantage of the acceleration feedback schema (b), which is that the steady-state error is zero even if the controller is a simple proportional gain, is only true for the calibrated plant. To handle the hardware differences an integral gain needs to be added and then, there is no benefit of using such a schema.

2.1. Wheel model

To take advantage of the knowledge of the system, a dynamic model of the wheel with the BLDC motor and the associated ESC is necessary. Reaction wheels are widely used and there are many models in the literature (see for example, (Hoevenaars et al., 2012; Carrara and Kuga, 2015; Muhamad et al., 2016). For a controller synthesis problem, the model should be representative (i.e., similar enough to the real system), but it is desirable to keep it as simple as possible to reduce the computation time and to be able to apply the well-known techniques for linear systems.

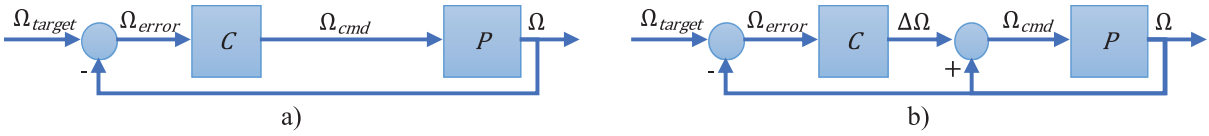

Fig. 4. Possible feedback schemas: implemented (a) and alternative (b).

Linear models for reaction wheels are usually built with a simplified monophasic equivalent electrical circuit and Newton's Second Law applied to the wheel. The first equation is then Kirchoff's Voltage Law extended with the back-EMF voltage (de Castro et al., 2018):

$$U = L\frac{dI}{dt} + IR + U_{BLDC} \tag{1}$$

where U is the PWM-controlled voltage, R and L are respectively the motor terminal resistance and inductance, I is the current drawn by the motor and its counter electromotive force (back EMF). U_{BLDC} is proportional to the rotational velocity ($U_{BLDC} = k_e\Omega$), being k_e the motor back-EMF constant. The second equation is a balance of the kinetic momentum of the wheel:

$$J\frac{d\Omega}{dt} = T_m - T_f \tag{2}$$

where J is the moment of inertia of the wheel and rotor, Ω is the angular velocity of the wheel, T_m is the torque applied to the motor and T_f is the friction torque. T_m is proportional to the electrical current ($T_m = k_m I$), where k_m is the motor torque constant. For T_f there are some different models depending on the application: for example (Khluabwannarat et al., 2020) uses a linearized aerodynamic model for multirotor, in (Zhou and Doyle, 1999) two 3rd order lineal systems are adjusted to represent the BLDC behavior and in (Bangura and Mahony, 2017) just a maximum value is used to assure the correct performance of the controller. In this work, as in (Desai and Emadi, 2005) and (Sathyan et al., 2009); T_f is modelled as proportional to the rotational velocity ($T_f = C_v\Omega$), where C_v is the motor dynamic friction coefficient. Therefore, the dynamics of the system can be expressed as a second-order Linear Time Invariant system (LTI):

$$\begin{aligned} L\tfrac{dI}{dt} &= U - IR - k_e\Omega \\ J\tfrac{d\Omega}{dt} &= k_m I - C_v\Omega \end{aligned} \tag{3}$$

or in its state space representation:

$$\begin{pmatrix} \frac{d\Omega}{dt} \\ \frac{dI}{dt} \end{pmatrix} = \begin{bmatrix} -\frac{C_v}{J} & \frac{k_m}{J} \\ -\frac{k_e}{L} & -\frac{R}{L} \end{bmatrix} \begin{pmatrix} \Omega \\ I \end{pmatrix} + \begin{bmatrix} 0 \\ \frac{1}{L} \end{bmatrix} U \tag{4}$$

Characterizing such a model implies knowing six parameters: C_v, J, k_m, k_e, L and R. A precise measurement of the inertia J requires disassembling the motor to consider the inertia of its rotor. For the small resistance R or inductance L of the BLDC motor, the measurement can be very difficult and getting precise values could require expensive equipment. k_e can be sometimes retrieved from the manufacturer, but C_v and k_m need some characterization tests. For example, in (Hoevenaars et al., 2012) a step response is used to adjust a model which also includes a static friction term. Nevertheless, as with any LTI state space representation, this model can be expressed as a transfer function in the frequency domain. This is more convenient for the controller design problem because all six parameters are grouped into only two: natural frequency ω_n and damping ratio ζ:

$$\frac{\Omega(s)}{\Omega_{cmd}} = \frac{\omega_n^2}{s^2 + 2\omega_n\zeta s + \omega_n^2} \tag{5}$$

Therefore, with a simple step response test it is possible to adjust the two parameters of the wheel. In Eq. (5), Ω_{cmd} is used instead of U, being:

$$\Omega_{cmd} = \frac{k_m U}{k_m k_e + RC_v} \tag{6}$$

Again, this characterization method is performed only once for one of the wheels that are used. The other wheels can be represented with this model simply by considering parameter variations as external disturbances managed with the use of the external controller. Some authors, (Carrara and Kuga, 2015; Hoevenaars et al., 2012), include the static friction in the friction torque model. In this work, those effects are also treated as external disturbances to maintain the generic model for all the wheels as simple as possible. In the experimental case, as the ESAT actuator is a momentum wheel (non-zero crossing), the linear model is accurate enough.

2.2. External controller structure

The structure of the controller in a state space implementation is:

$$\begin{cases} \dot{p} = Kp + L\Omega_{error} \\ \Omega_{cmd} = Mp + N\Omega_{error} \end{cases} \tag{7}$$

where p is the controller state vector, Ω_{error} is the error signal closing the loop ($\Omega_{error} = \Omega_{target} - \Omega$), Ω_{cmd} is the output of the controller (see Fig. 4), and K, L, M and N are 2x2 real matrixes tuned by the controller synthesis method described later.

The transfer function of Eq. (7) is:

$$\frac{\Omega_{cmd}}{\Omega_{error}} = M(sI - K)^{-1} + N \tag{8}$$

The proposed methodology allows to synthesize a linear controller of any size (number of states) and bandwidth extending the design possibilities to any hardware used; but it can also be used to tuned fixed structures like the PI or PID in a procedural way and with a robust point of view. So, in this work a PID controller will be used.

A simple PID ($\frac{\Omega_{cmd}}{\Omega_{error}} = K_p + K_i s^{-1} + K_d s$) cannot be expressed as a state space without a mass matrix as it is not a proper system with more poles than zeros as Eq. (8). It can be seen by expanding Eq. (8), that the order of the denominator of the transfer function is related to the determinant of $sI - K$ and the numerator has one order less if $N = 0$, due to the adjoint of the matrix, or the same order as the denominator if $N - 0$:

$$M(sI-K)^{-1} + N = M \cdot \frac{Ad(sI-K)'}{|sI-K|} + N = \\ = \frac{M \cdot Ad(sI-K)' + N|sI-K|}{|sI-K|} \tag{9}$$

Although a PI should be enough to control a reaction wheel (see section 3), to have a more general controller without additional constraints on its structure, a first-order low-pass filter is included in the derivative term so that there is one more pole and the number of poles equals the number of zeros. Note that this introduces a new tunable gain: the filter time constant, T_d. Such a filter is commonly used because it also reduces the possible numerical noise of the derivative term. So, the implemented PID is:

$$\frac{\Omega_{cmd}}{\Omega_{error}} = K_p + \frac{K_i}{s} + \frac{K_d s}{T_d s + 1} \tag{10}$$

In this case, the PID can be expressed in a state space form as in Eq. (7). The controllable canonical form is used:

$$K = \begin{bmatrix} 0 & 1 \\ 0 & -\frac{1}{T_d} \end{bmatrix} \\ L = \begin{bmatrix} 0 \\ 1 \end{bmatrix} \\ M = \begin{bmatrix} \frac{K_i}{T_d} & K_i - \frac{K_d}{T_d^2} \end{bmatrix} \\ N = \left[K_p + \frac{K_d}{T_d} \right] \tag{11}$$

The eigenvalues of the Linear Time Invariant (LTI) system in Eq. (11) are 0 and $1/T_d$. Therefore, the filter time constant is the characteristic time of the controller too, i.e., T_d is a good estimation of the order of magnitude of the integration step time and, thus, the controller/processor velocity requirements.

2.3. Tuning method

Once the controller structure is defined, the gains need to be tuned to obtain a robust controller which works for every satellite avoiding a dedicated calibration. The problem is treated as a disturbance rejection problem where the calibration errors are introduced as the external disturbances. The gains are computed in an H_∞ synthesis problem with the additional constraint on the controller structure defined in Eq. (11). The algorithm detailed in (Apkarian and Noll, 2006) presents a schema to solve such H_∞ problems under additional structural constrains, and it is therefore used in this work. The schema in Fig. 4 needs to be augmented to include some weighting functions and, thus, define the objectives of the closed loop for the optimization process. The augmented model used is shown in Fig. 5. The design proposed in this work absorbs the errors due to calibration through an external disturbance, Ω_{noise}, and its weighting function W_{noise}, which represents a bound to the expected error spectrum produced by using the same calibration curve for all the wheels instead of a dedicated one for each wheel. As this is a steady state error, a very low bandwidth should be selected. The magnitude of this error depends on the differences in the design and manufacturing of the different wheels, as described in the introduction. So, with this new design, the input to the calibration process (which uses the same curve for all the wheels) is $\Omega_{cmd} + W_{noise}\Omega_{noise}$, instead of Ω_{cmd}, which is the input in the speed feedback control used in previous works for an individual wheel. The H_∞ controller is synthesized to reject that external noise.

The transfer matrix from the reference input signal $(\Omega_{target}, \Omega_{noise})$ to the output vector $\boldsymbol{z} = (z_e, z_{cmd})$ in the augmented model, G, is:

$$G = \begin{bmatrix} W_e \left(P_{desired} - \frac{PC}{1+PC} \right) W_{target} & -W_e \frac{P}{1+PC} W_{noise} \\ W_{cmd} \frac{C}{1+PC} W_{target} & -W_{cmd} \frac{CP}{1+PC} W_{noise} \end{bmatrix} \tag{12}$$

where P corresponds to Eq. (5) and C to Eq. (10).

The function to optimize is the H_∞ norm of this transfer matrix:

$$\|G\|_\infty = \sup \sigma_1 [G(j\omega)]_{\omega \in \mathbb{R}} \tag{13}$$

where σ_1 is the largest singular value.

The inputs Ω_{target} and Ω_{noise} are shaped with the weighting functions W_{target}, which represents the reference commanding signal dynamics,and W_{noise} to normalize them and to capture the magnitude, M, and bandwidth, b, of those signals. This is done through a first-order filter:

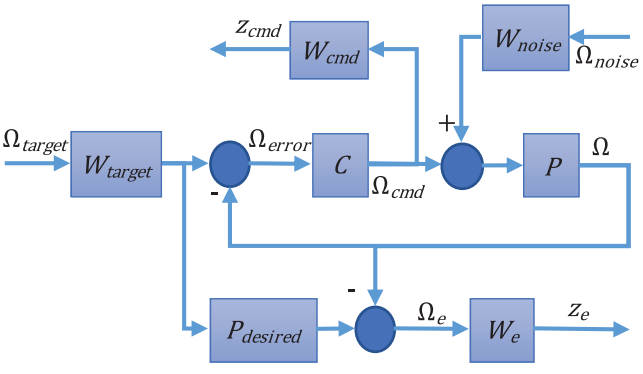

Fig. 5. Augmented model.

$$W_{target} = \frac{M_{target}}{\frac{s}{2\pi b_{target}} + 1}, W_{noise} = \frac{M_{noise}}{\frac{s}{2\pi b_{noise}} + 1} \quad (14)$$

$P_{desired}$ is the desired behaviour of the closed loop of the plant, P, and the controller, C. Ideally, Ω should be equal to Ω_{target} but, as this is not possible due to the dynamics of the plant, a second order linear system similar to Eq. (5) is used to define a realistic objective of how the transfer function from Ω_{target} to Ω should be:

$$\frac{\Omega(s)}{\Omega_{target}} = \frac{\omega^2_{n_{desired}}}{s^2 + 2\omega_{n_{desired}}\zeta_{desired}s + \omega^2_{n_{desired}}} \quad (15)$$

The objectives, thus, can be expressed in the frequency domain in terms of a natural frequency and damping ratio desired for the closed loop and can be computed from the time domain for some desired peak response, settling time, rise time and/or steady state error.

Therefore, the error to be minimized is the difference between the output of $P_{desired}$ and the output of the wheel with the controller, i.e., Ω. The weighting function W_e is included to assure a good reference tracking at low frequencies. In effect, as it will not be physically possible to track references with high frequencies, W_e penalizes only low ones. So z_e is the weighted difference between the objective wheel velocity response and the real one. In the same way W_{cmd} is used to avoid solutions with high frequencies in the control signal. As the plant will act as a filter for these high frequencies, it makes no sense to waste energy commanding in that way, and W_{cmd} will penalize only high frequencies. Thus, z_{cmd} is the weighted control effort. These functions are selected taking into account the recommendations in (Zhou and Doyle, 1999):

$$W_e = \frac{\beta}{M_{target}} \frac{\frac{s}{M_e} + \omega_e}{s + \omega_e \varepsilon_e} \quad (16)$$

$$W_{cmd} = \frac{(1-\beta)}{M_{target}} \frac{s + \frac{\omega_{cmd}}{M_{cmd}}}{\varepsilon_{cmd}s + \omega_{cmd}} \quad (17)$$

where M_e is related with the overshoot objective (or, conversely, the damping ratio), ε_e is the maximum steady state error allowed for the closed loop, and ω_e is the desired signal tracking bandwidth. Similarly, M_{cmd} is the maximum control gain, ω_{cmd} is the controller bandwidth and ε_{cmd} is the control signal high frequency attenuation. β is used to weigh the importance of the objectives: to penalize the high frequency components in the control signal ($\beta \cong 0$) or to penalize the low frequency components in the error signal ($\beta \cong 1$). M_{target} has been added in both filters to normalize the output. Therefore, the parameters present in the weighting functions modify the desired objectives for the closed loop making them reasonable for a realistic implementation in case what is defined in $P_{desired}$ is unreachable due to the necessity of an unrealistically fast processor to make it possible.

3. Experimental tests

Experimental results have been obtained with the reaction wheels of seven laboratory satellite ESATs (Theia Space, 2023) manufactured in a timeframe of two year with hardware differences. ESAT is a laboratory satellite (see Fig. 6) used in many universities and research centers to test on ground several concepts related to CubeSats (Salgado Sánchez et al., 2021; Bello et al., 2023). As part of its ADCS, it is equipped with a momentum wheel to control the satellite orientation in the vertical axis. All manufactured units undergo a series of tests before their acceptance, one of which is the calibration of the ESC controlling their wheel speed. Hence, the external controller proposed in this work will be used to handle the differences between the ESAT wheels, thus avoiding the need for an individual ESC calibration for each ESAT.

ESAT ESC follows the schema presented in Fig. 2. The implemented ESC is the widely used schema consisting of an H-bridge per phase (e.g. (Aydin et al., 2010)). Fig. 7 shows the ADCS board with a simplified schema of the ESC implemented. The feedback is based in the back EMF by passing the three output phases through resistor dividers (to bring the voltage down between 0 and the power bus line, in this case, 5V), and then are connected to ADC (Analog to Digital Converter) processor channels.

3.1. The calibration curve

As already mentioned, the wheel is commanded via PWM. Nevertheless, all the attitude calculations on board

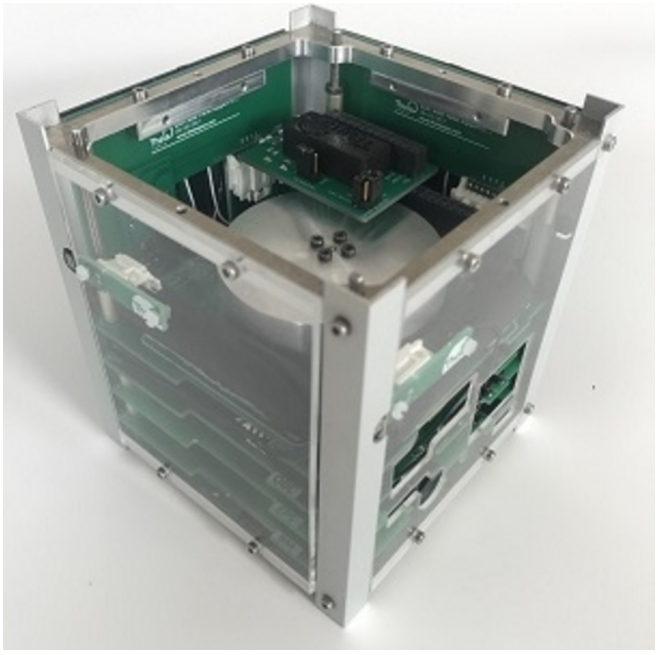

Fig. 6. ESAT.

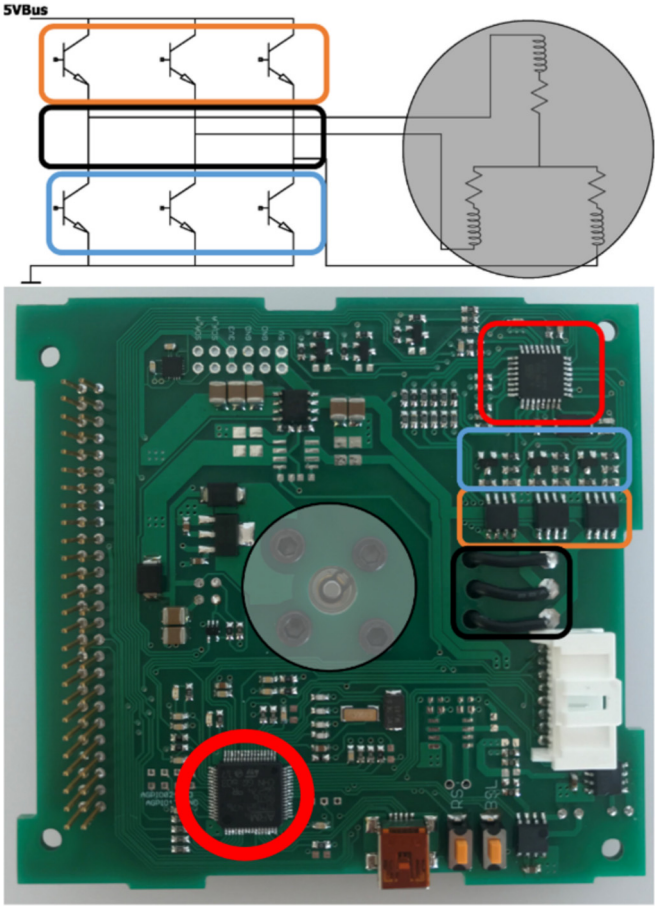

Fig. 7. ESAT ADCS board with the ESC and the external controller highlighted. The external controller is marked with the red circle and the processor in charge of the phase commutations (transistors turned on/off) is marked with the red square.

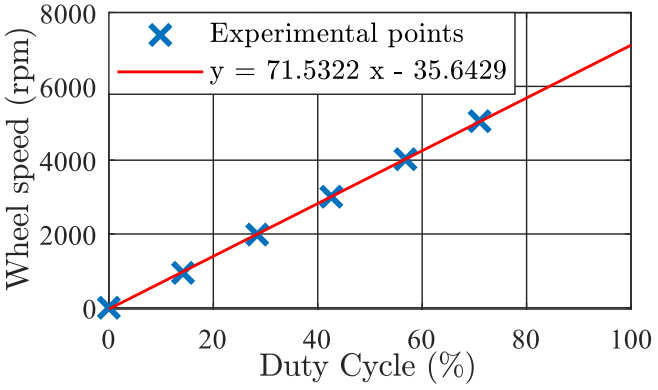

Fig. 8. Experimental calibration curve.

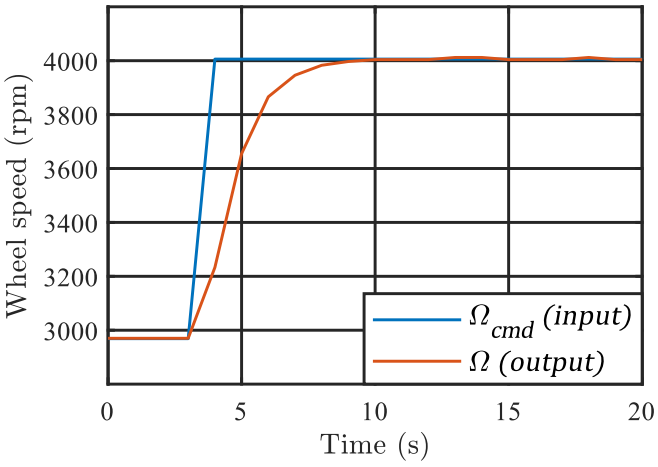

Fig. 9. Step response test performed with an ESAT.

are made with the angular velocity of the wheel, so a calibration curve which relates the commanded PWM with the angular velocity of the wheel is necessary to implement the attitude controller in the ADCS processor. The objective of this paper is to make unnecessary having one calibration curve for each satellite, but an initial one needs to be measured. Once the robust external controller is computed, the same generic calibration curve should work properly for all the wheels and through the lifecycle of the satellites.

By commanding some PWM duty cycles and waiting for the steady state response of one wheel on one single ESAT, one can fit the resulting data with a linear regression as shown in Fig. 8.

Fig. 8 shows that, although ideally the calibration curve should not have an independent term, it appears due to the factors described in the introduction. Both the linear fit slope and the independent term vary slightly from one wheel to another, so the calibration curve will be different. The use of the external controller, allowing all ESATs to use the calibration curve in Fig. 8 along their complete lifetimes, would therefore greatly reduce the development and testing time.

3.2. Wheel model adjustment

The simple wheel model proposed in section 2.2 needs to be accurate enough to reproduce the behaviour of the wheel for the controller synthesis problem.

As has been explained in that section, a step response test can be used to characterize such a model. In this work a test has been performed with the previously calibrated ESAT wheel (from section 3.1), using an initial velocity of 3000 rpm, a commanded input step of +1000 rpm, and the calibration curve in Fig. 8. These step values were selected because they are characteristic of ESAT operations. Fig. 9 shows the resulting time evolution of the wheel speed (commanded and measured) during this step response test.

The commanded input data recorded in the ESAT telemetry during the test (Ω_{cmd}(input) in Fig. 9) is used now to feed the mathematical model (Ω_{cmd} in Eq. (5)). Then the model is integrated, and the output is calculated for some initial values of ω_n and ζ. The simulated output (Ω_{sim}) is evaluated at the same time points of the ESAT telemetry recordings (Ω(output) in Fig. 9), i.e., each second. We define the cost function *Cost* to measure the differ-

ence between the measured response, Ω(output), and the simulated one, Ω_{sim}:

$$Cost = \sum_{i=1}^{n} [\Omega(i) - \Omega_{sim}(i)]^2 \quad (18)$$

where i is each time step and n is the total number of measurements recorded in the ESAT telemetry. $\Omega(i)$ is the i-th recorded value of $\Omega(output)$.

Adjusting the model consists of varying its parameters, ω_n and ζ, to minimize the *Cost* function. This minimization has been carried out with a trust region algorithm (Coleman, 1994; Coleman, 1996), and the values obtained are presented in Table 1, along with those of the weighting functions' parameters, which are explained in the next section:

The simulated response using these values can be compared with the measured response to check if the adjusted model is representative (see Fig. 10):

It can be concluded that the generic second order system is suitable for the controller synthesis problem because it is simple, representative (Cost function = 2e-5 rpm^2) and allows one to use well-known analysis and synthesis techniques for linear systems.

3.3. Weighting functions selection

Next, appropriate parameter values for the weighting functions in Eq. (14) are selected. M_{target} is set to 1000 rpm as a typical order of magnitude for the ESAT wheel speed, and b_{target} is selected to be 1 Hz, because that is the ESAT ADCS control loop frequency.

As previously mentioned, b_{noise} should be low because, in fact, the error is a steady state error. It has been set two orders of magnitude lower than the reference commanding signal, $b_{noise} = 0.01$ Hz. From previous experience working with ESATs, the difference between the wheel velocities obtained in different ESAT units when commanding the same PWM can be about 200 to 300 rpm. To have some margins and be sure that the controller will be able to manage all the wheels, M_{noise} is set to 500 rpm.

Table 1
Wheel model parameter values.

P	ω_n	2.3834 rad/s
	ζ	1.5814
W_{target}	M_{target}	1000 rpm
	b_{target}	1 Hz
W_{noise}	M_{noise}	500 rpm
	b_{noise}	0.01 Hz
W_e	β	0.7
	M_e	1.15
	ω_e	0.5Hz = πrad/s
	ε_e	0.001
W_{cmd}	M_{cmd}	1.15
	ω_{cmd}	0.5Hz = πrad/s
	ε_{cmd}	0.001
$P_{desired}$	$\omega_{ndesired}$	3 rad/s
	$\zeta_{desired}$	1.5814

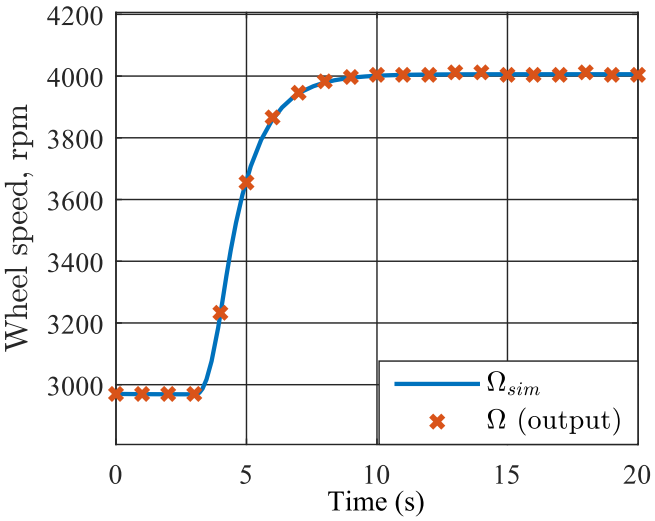

Fig. 10. Comparison of the experimental and simulated outputs.

As can be seen in Fig. 10, the transient response of the wheel in open loop is good enough. Therefore, $P_{desired}$ can be generated with the same values for ω_n and ζ obtained in section 3.2 (see Eq. (15)). Although the primary objective of the external controller is to avoid a different calibration curve for each wheel, it is also possible to achieve a better performance of each wheel transient response. In the case of the ESAT the open loop response is well damped: overdamped (no undesired oscillations) with a damping ratio near 1 (not to increase the steady state time). Therefore, the damping ratio, $\zeta_{desired}$, is left as in the characterization, ζ, but the natural frequency, $\omega_{ndesired}$, is increased with respect to the open loop wheel ω to 3 rad/s to reduce the settling time about one second (from 4.77 to 3.77 s).

The components of W_e and W_{cmd} (Eqs. (16) and (17)) are selected as follows:

(i) M_e is related with the dumping ratio (see (Zhou and Doyle, 1999), and a value of 1.15 is selected to have a dumping ratio near 1.
(ii) The bandwidth is necessarily selected a little bigger than the $P_{desired}$ bandwidth, with a value of 0.5 Hz.
(iii) $\varepsilon_e = 0.001$ is selected to allow a maximum of 0.1 % steady state error, which is smaller than the noise in the wheel velocity signal.
(iv) M_{cmd}, ε_{cmd} and ω_{cmd} are set to the same values as M_e, ε_e and ω_e, and β is set to 0.7 to favour reference tracking and disturbance rejection over the control effort.

Fig. 11 shows the final shape of the weighting functions. W_e penalizes only the low-frequency errors (as a high frequency reference is not possible to be tracked) and W_{cmd} penalizes only the high-frequency commands, as the low ones are needed to follow the reference signal.

3.4. Optimization results

Once all the model parameters are set, the steepest descent method described in (Apkarian and Noll, 2006), and

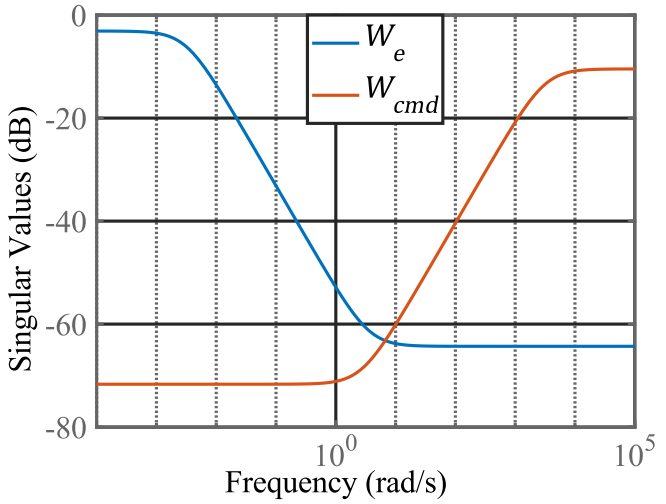

Fig. 11. W_e and W_{cmd} shapes.

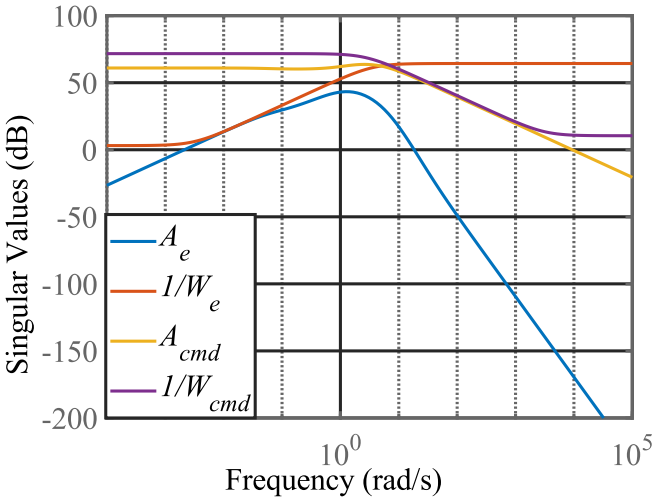

Fig. 12. Optimization results.

already implemented in MATLAB®, is used to calculate the PID gains in Eq. (10). This method searches for the values of the controller variables (Eq. (10)) which minimize the H_∞ norm of $G(s)$: $\|G\|_\infty$ (Eqs. (12) and (13)). This non-smooth optimization has been executed 100 times with different random initial values of the controller gains, obtaining a minimum H_∞ norm of 0.9922 with the controller values shown in Table 2.

The H_∞ norm value lower than 1 indicates that all the objectives were accomplished. To check this, it is possible to define two auxiliary systems A_e and A_{cmd}, such that:

$$z_e = W_e A_e \begin{bmatrix} \Omega_{target} \\ \Omega_{noise} \end{bmatrix}$$

$$z_{cmd} = W_{cmd} A_{cmd} \begin{bmatrix} \Omega_{target} \\ \Omega_{noise} \end{bmatrix}$$

They are obtained from Eq. (12):

$$A_e = \begin{bmatrix} \left(P_{desired} - \frac{PC}{1+PC}\right) W_{target} & -\frac{P}{1+PC} W_{noise} \end{bmatrix}$$

$$A_{cmd} = \begin{bmatrix} \frac{C}{1+PC} W_{target} & -\frac{CP}{1+PC} W_{noise} \end{bmatrix}$$

Fig. 12 shows how the weighting functions W_e and W_{cmd} shape the input–output relationships A_e and A_{cmd}, specially near the crossover frequencies. W_e penalizes the low frequency tracking errors, so the maximum singular value of A_e remains below $1/W_e$ at low frequencies. The same applies to W_{cmd}: the commanding signal is attenuated below $1/W_{cmd}$ at high frequencies. Moreover, as the minimum $\|G\|_\infty$ obtained in the optimization is less than 1, the singular values of A_e and A_{cmd} are, respectively, below $1/W_e$ and $1/W_{cmd}$ throughout all the spectrum.

Table 2
PID gains from optimization.

K_p	K_i	K_d	T_d
1.68	1.17	−3.38	17.7

A secondary objective of the external controller is to improve the response of the system by reducing the settling time with respect to the open loop. As the H_∞ norm is less than 1, the closed loop is expected to behave more akin to the reference system, $P_{desired}$. Fig. 13 shows the step response for the original open loop, $P_{desired}$, and for the closed loop obtained after the optimization. It can be seen that the final closed loop is even better than the desired objective. The settling times for the open loop, the desired plant and the closed loop are, respectively, 4.77, 3.78 and 3.1 s.

3.4.1. About the controller structure

Looking at the controller gain values in Table 2, it seems that a complete PID controller is not needed, and a PI control could be enough, as the value of K_d/T_d is one order of magnitude smaller than K_p or K_i . Repeating the optimization with this new constraint leads to the same minimum

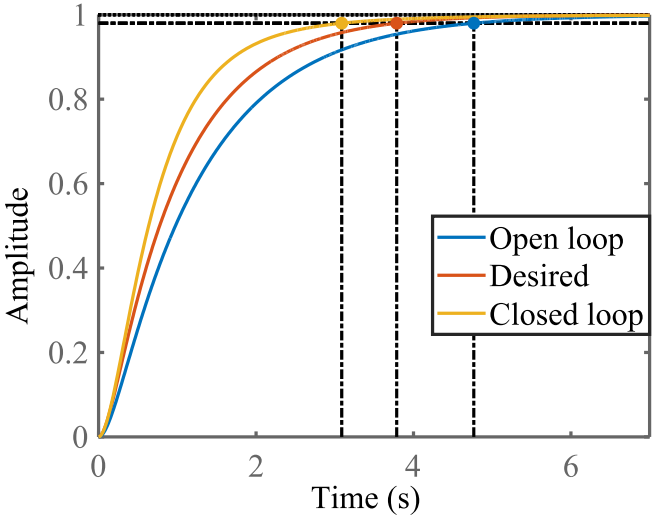

Fig. 13. Step response with settling times.

H_∞ norm of 0.9922. Thus, the objectives can indeed be accomplished with a PI controller with very similar results as with the PID. The gains obtained for this PI are also quite similar: $K_p = 1.66$ and $K_i = 1.17$. Bode diagrams of both controllers are represented in Fig. 14, showing that both are quite similar.

The method proposed in this paper allows to synthetize a full order H_∞ controller. For ESAT, the complete PID is maintained to allow the final user to make adjustments if desired, but in performance terms it seems unnecessary, and the simpler PI version would also work well.

3.5. Experimental test results

To check if the assumptions made in the analytical approach to this problem are accurate, the obtained controller has been implemented in a set of seven ESATs manufactured in a timeframe of two years, which present slight differences in hardware (for example, the on-board processor is different between older and newer units). The external controller has been implemented as a state space (as described in section 2.3) and integrated through the trapezoidal rule at a rate of 4 Hz. All ESATs use the same calibration curve, calculated in section 3.1 (see Fig. 8).

Fig. 15 shows the results of a step response test with each ESAT, commanding their wheels from 1000 to 2000 rpm. All the wheel speed curves show nearly the same response, proving that the controller is able to handle the differences between ESATs and make them work in the same way. There is one curve with a slight overshoot (6.5 %), but it does not affect the overall functionality of this ESAT and is still an acceptable result. The overshoot of the rests of wheels remains below 3.5 %.

The differences between ESATs can be appreciated particularly in the PWM duty cycle signal commanded to obtain each wheel speed response. The differences in the steady state duty cycle are about 3 %, which represents

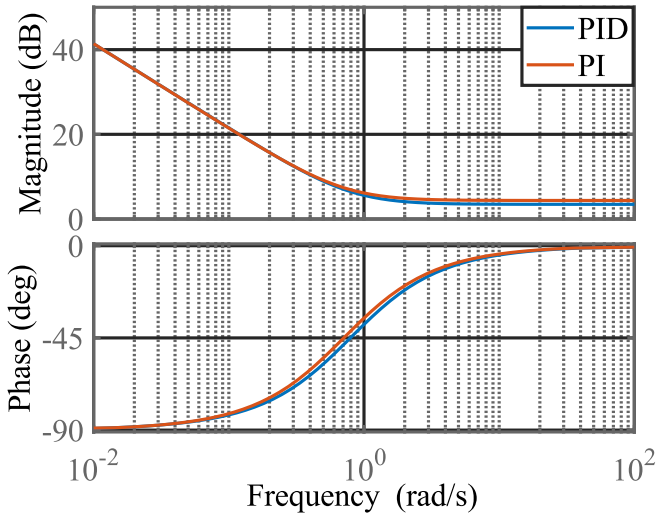

Fig. 14. Bode diagrams of the proposed PI an PID.

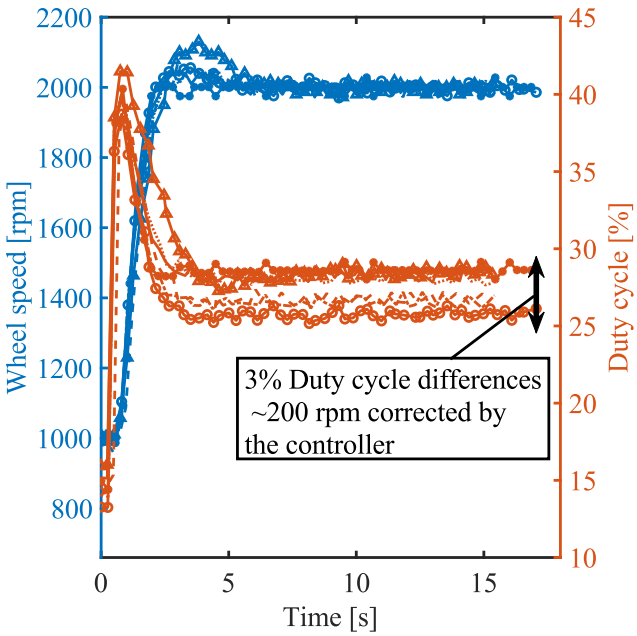

Fig. 15. ESAT tests results.

an error (in open loop) of around 200 rpm that should be handled with a dedicated calibration curve if the external controller was not present. The controller was designed for a nominal disturbance amplitude of 500 rpm ($M_{noise} = 500$), therefore, it should be able to handle more than the double of the real (measured) errors coming for the absence of a calibration curve.

Regarding the steady state error, all wheels show one below 0.1 %, which was another design objective ($\varepsilon_e = 0.001$).

4. Robustness with respect to uncertainty in the model

The present work deals with the differences between wheels and calibration curves by adding an external disturbance in the augmented model (see Fig. 5) and synthesising an H_∞ controller to reject it. One could treat this problem trying to represent all the wheels and calibration curves by adding some uncertainty in the ω_n and ζ values of the generic model (Eq. (5)) and synthesising a robust controller which minimizes the effect of uncertainty in the performance of a feedback loop, i.e., minimizes the maximum structured singular value μ (Doyle, 1982). However, this approach does not cover the calibration error problem. An error in the calibration curve produces a steady state error which is easily represented with an external disturbance added to the command signal. Varying ω_n and ζ values will not reproduce such behaviour and, therefore, the introduction of the external disturbance in the augmented plant will still be necessary.

Nevertheless, considering some uncertainty in the model parameters could still be useful to obtain a robust controller against model uncertainties. To check this, a ± 20 % of uncertainty has been added to both model

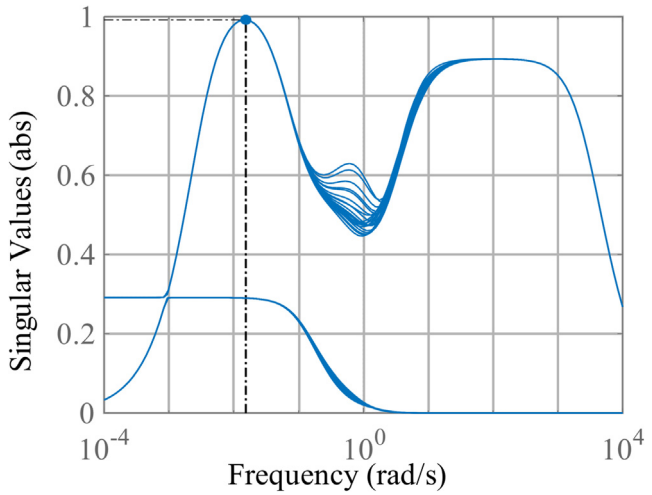

Fig. 16. $G(s)$ singular values obtained in Montecarlo simulation.

parameters and the procedure described in section 3.4 has been repeated for a uniform distribution of points (ω_n, ζ) in the uncertainty interval. The results of a Montecarlo analysis for this uncertainty are shown in Fig. 16, where the singular values of the whole augmented plant are represented.

The low frequency maximum singular value of $G(s)$ is related with the minimization of the steady state error, where A_e is closest to $1/W_e$. This is where the minimum H_∞ (0.9922) achieved for $G(s)$ is reached. The higher frequency local maximum is related to the second objective of avoiding high frequencies in the control signal, where A_{cmd} is closest to $1/W_{cmd}$. The difference between this local maximum and the global one can be reduced by reducing the β parameter in the weighting functions W_e and W_{cmd}. In any case, the uncertainty added in the model does not affect any of the maxima and thus, does not affect the minimum achievable H_∞ norm. Therefore, it brings no benefits to add it and to perform a minimization of the μ value. Naturally, with a higher uncertainty a new maximum could appear in the frequency region affected by the uncertainty, but for the ESAT such big uncertainty is not realistic.

5. Conclusions

The main objective of this work is easing the management of the performance of multiple reaction wheels in space missions along their life cycle, avoiding a specific calibration (and possible recalibrations) of each wheel in the mission, for which, a robust controller is designed and experimentally verified.

A new H_∞ control design concept has been presented detailing a procedure for the weighting functions and parameters selection, avoiding the usual iterative search of parameters and filters for the most appropriate weighted H_∞ norm definition. The methodology allows to synthesize a linear controller of any size (number of states) and bandwidth extending the design possibilities to any hardware used so that the hardware restrictions (bandwidth and memory) can be taken into account in the design process; but it can also be used to tuned fixed structures like the PI or PID in a procedural way and with a robust point of view.

In this design method the calibration variations are formulated as a disturbance rejection problem: the steady state errors introduced by the absence of a dedicated calibration curve are treated in the augmented model, as a low frequency external noise, that is added to the command signal, with its corresponding weight function, so the input to the calibration process (which uses the same curve for all the wheels) is the command signal plus the noise signal, instead of the command signal, which is the input in the speed feedback control used in previous works for an individual wheel.

It is important to point out that, although physically the problem is an uncertainty of the model, an error in the calibration curve produces a steady state error, which behaviour could not be reproduced by including uncertainties in the wheel model and, therefore, the introduction of the external disturbance in the augmented plant will still be necessary.

The obtained controller has been implemented in various ESATs manufactured in a timeframe of two year with hardware differences and an experimental test campaign has been performed. The methodology used to calculate the parameters in the noise weight function is easily extensible to any other problem. The experimental results show that the external controller presented in this work can handle the hardware differences using a single calibration curve for all the wheels. These differences have been measured and can be up to 200 rpm (10 % steady-state error). What is more, the simulations show that the external controller presented here should be able to handle up to 500 rpm (more than the double of the real differences), in addition to improving the response of the wheel with the ESC, in terms of settling and rise times. The controller used in this empirical example is tuned through a H_∞ norm minimization algorithm for fixed structure controllers, in this case a PID, although the method can be also used for a general linear controller without structural constraints.

The general approach of the developed method as a disturbance rejection problem has been compared with an approach seeking for robustness against uncertainty. In this case, the analysis concludes that adding reasonable levels of uncertainty to the nominal model of the reaction wheel would not affect the frequency regions where the objectives of the H_∞ norm minimization were defined, therefore not affecting the optimization results, and making this addition unnecessary in practical terms.

Finally, note that the methodology presented here is extensible to any application where multiple BLDC motors are used, and individual calibrations are to be avoided.

Declaration of competing interest

The authors declare that they have no known competing financial interests or personal relationships that could have appeared to influence the work reported in this paper.

References

Apkarian, P., Noll, D., 2006. Nonsmooth H∞ synthesis. IEEE Trans. Autom. Control 51 (1), 71–86.

Aydin, M., Huang, S., Lipo, T.A., 2010. Design, analysis, and control of a hybrid field-controlled axial-flux permanent-magnet motor. IEEE Trans. Ind. Electron. 57 (1), 78–87.

Bangura, M., Mahony, R., 2017. Thrust control for multirotor aerial vehicles. IEEE Trans. Rob. 33 (2), 390–405.

Bello, Á., del Castañedo, Á., Olfe, K.S., Rodríguez, J., Lapuerta, V., 2021. Parameterized fuzzy-logic controllers for the attitude control of nanosatellites in low earth orbits. A comparative studio with PID controllers. Expert Syst. Appl. 174 114679.

Bello, A., Olfe, K.S., Rodríguez, J., Ezquerro, J.M., Lapuerta, V., 2023. Experimental verification and comparison of fuzzy and PID controllers for attitude control of nanosatellites. Adv. Space Res. 71, 3613–3630.

Burakov, M.V., Krivolapchuk, I.G., Shishl, V.F., 2019. Fuzzy control of spacecraft reaction wheel. Gyroscopy Navig. 10 (4), 339–345.

Carrara, V., Kuga, H., 2015. Current and speed control operating modes of a reaction wheel. Appl. Mech. Mater. 706, 170–180.

Coleman, T.F., Li, Y., 1996. An interior, trust region approach for nonlinear minimization subject to bounds. SIAM J. Optim. 6, 418–445.

de Castro, A.G., Pereira, W.C.A., de Almeida, T.E.P., de Oliveira, C.M. R., de Almeida Monteiro, C.R.B., 2018. Improved finite control-set model-based direct power control of BLDC motor with reduced torque ripple. IEEE Trans. Ind. Appl. 54 (5), 4476–4484.

Desai, P.C., Emadi, A., 2005. A novel digital control technique for brushless DC motor drives: current control. In: IEEE International Conference on Electric Machines and Drives, San Antonio, TX, USA.

Doyle, J., 1982. Analysis of feedback systems with structured uncertainties. IEE PROC, vol. 129.

Fatimi, A.E., Addaim, A., Guennoun, Z., 2022. Real-time software in the loop simulation for PID control of the nanosatellite reaction wheel. In: 2nd International Conference on Innovative Research in Applied Science, Engineering and Technology (IRASET). IEEE publisher.

Ge, S., Cheng, H., 2006. A comparative design of satellite attitude control system with reaction wheel. In: Proceedings of the First NASA/ESA Conference on Adaptive Hardware and Systems.

Hoevenaars, T., Engelen, S., Bouwmeester, J., 2012. Model-based discrete PID controller for cubesat reaction wheels based on cots brushless DC motors. Adv. Astronaut. Sci. 145, 379–394.

Khluabwannarat, P., Nawikavatan, A., Puangdownreong, D., 2020. Application of parallel flower pollination algorithm to fractional-order model identification of BLDC motor. In: 17th International Conference on Electrical Engineering/Electronics, Computer, Telecommunications and Information Technology (ECTI-CON), Phuket, Thailand.

Li, Y., Coleman, T.F., 1994. On the convergence of reflective newton methods for large-scale nonlinear minimization subject to bounds. Math. Program. 67, 189–224.

Lobanov, V.S., Tarasenko, N.V., Zboroshenko, V.N., 2016. Orientation and stabilization systems of space vehicles for different purposes: Lines of development. Gyroscopy Navig. 7 (1), 50–57.

Muhamad, N.N., Susanto, E., Syihabuddin, B., Wibawa, I.P.D., 2016. Reaction wheel control design using linear quadratic controller, Yogyakarta, Indonesia.

Navabi, M., Hosseini, M.R., 2017. Spacecraft quaternion based attitude input-output feedback linearization control using reaction wheels. In: 8th International Conference on Recent Advances in Space Technologies (RAST), Istanbul, Turkey, pp. 97–103.

Salgado Sánchez, P., Tinao, I., Ezquerro, J.M., Fernández, J.J., Rodríguez, J., Bello, Á., Olfe, K., 2021. Educational nanosatellites for hands-on learning in. In: Proceedings of INTED2021 Conference, Valencia (Spain).

Sathyan, A., Krishnamurthy, M., Milivojevic, N., Emadi, A., 2009. A low-cost digital control scheme for Brushless DC motor drives in domestic applications. In: IEEE International Electric Machines and Drives Conference, Miami, FL, USA.

Sidi, M.J., 2014. Spacecraft Dynamics and Control. A Practical Engineering Approach, Israel Aircraft Industries Ltd. and Tel Aviv University. https://doi.org/10.1017/CBO9780511815652.

Theia Space, ESAT brochure, 2023. Available in: http://www.theiaspace.com/ products/.

Zhou, K., Doyle, J., 1999. Essentials of Robust Control. Prentice Hall.